Fermi National Accelerator Laboratory

FERMILAB-Pub-82/62-EXP
7552.623

THE E623 $\phi\phi$ TRIGGER PROCESSOR

H. C. Fenker, D. R. Green, and S. Hansen
Fermi National Accelerator Laboratory, Batavia, IL 60510

and

T. F. Davenport
Florida State University, Tallahassee, FL 32306

September 1982

Operated by Universities Research Association Inc. under contract with the United States Department of Energy

ABSTRACT

A fast (200 nanosecond) hardware processor for recognizing tracks in high energy physics experiments and computing kinematic quantities from their momenta and production angles is described. The system was used to form the trigger in an experiment run recently at Fermilab. Its performance is studied in the context of this experiment.

I. Introduction

An experiment (E-623) has been performed at the Fermilab Multiparticle Spectrometer (MPS) to search for states decaying to two ϕ mesons. Crucial to this experiment was the design and operation of a high speed processor which seeks events containing at least two pairs of opposite charge kaons which have an effective mass compatible with the ϕ mass. This paper describes the processor.

The system which was constructed is rather general in that it is basically a track finder which determines momentum and production angle, and a measurer of detector multiplicity. This information is needed for most types of topological/kinematical triggers. A small, experiment dependent part of the electronics chooses which found tracks to process and computes kinematic quantities involving them. For example, effective mass and transverse momentum may be calculated.

This system is cheap ($\sim$20 K$) and fast (trigger decision within 150 ns). It is competitive with more expensive, slower ($\sim$ 10 μs), but higher resolution single wire processors.

II. Physical Description

The system is composed of both Fermilab designed and commercial electronics (see Fig. 1). Signals are pre-amplified and logically ORed at the multiwire proportional chambers (P1, P2, P3) by Fermilab designed electronics and sent to

receiver/latches as differential ECL pulses. Phototube signals from the multicell Cerenkov counters (C1, C2) and scintillator hodoscope (H1) are discriminated in standard NIM modules. These NIM pulses are also sent to Fermilab designed latches. For each particle interaction the data is latched and sent to the processor as single-ended transmissions on wire-over-ground multiconductor ribbon cable.

The core of the processor resides in a crate manufactured by MUPAC [1] which supports both wire-wrap cards and backplane having very good ground plane and power distribution characteristics. Most of the system logic is implemented on these cards which, given some care in wire routing, provide an adequate environment for the ECL-10000 signals.[2] The use of the wire wrap technique has been found to be quite beneficial in that logic modifications are simple and the processor can be reprogrammed very rapidly.

The latched data are also sent to Fermilab designed window discriminators for multiplicity cuts, and to commerical CAMAC modules which store all of the trigger data for readout to magnetic tape.

III. Track Recognition Logic

As shown in Fig. 1, the detectors used in the trigger decision are three proportional wire chambers P1, P2, P3, two threshold Cerenkov counters C1 and C2, and a scintillator hodoscope wall, H1. Each of these detectors is divided into 32

elements for triggering purposes.

A track is defined as a coincidental hit in all three elements of a predefined "road" through P1, P2, and P3. A point target plus these three points provides redundant four point tracking. The coincidences are all performed in parallel rather than by looping over arrays of hits. This parallel processing accounts for the speed of the track finding algorithm. Each road is uniquely identified by its XZ plane (magnet bend plane) production angle θ and momentum P. The production angle is given by the cell number in P1(0-31). The inverse momentum, $S \equiv 1/P$, is measured as the difference, in units of P3 cells, between where the particle struck P3 and where a particle with infinite momentum and production angle θ would have struck P3. As shown in Fig. 2, the logic is arranged so that two neighboring elements of P2 are used in each "road." This compensates for the finite sizes of the beam, target, and detector hodoscopes.

It should be noted that the non-bend plane component of the production angle could be measured by means of a straight-forward addition to the above logic. For example, a redundant y measurement at P3 for each struck element in P3 would be provided by a coincidence involving two slant planes near this detector:

$$H(p,\theta,\theta_y) = P3_{j(p,\theta)} \cdot P3U_{m(j,\theta_y)} \cdot P3V_{n(j,\theta_y)}.$$

This additional information would require additional fast or amplifiers, latches, and another MUPAC crate ($\sim$ 10 K$). The measurement would be accessed in the same way that the momentum is retrieved from the road logic. Such a scheme was not implemented in this particular experiment since the processor reduced the trigger rate to an acceptable level in the presence of the maximum beam flux that the detectors could tolerate.

The kind of road definition used is quite efficient for finding tracks. Only when two tracks traverse exactly the same road is one of them "missed." In a sample of Monte Carlo events having a mean multiplicity of eight, about 1% of the tracks within a momentum range of 6 to 22 GeV/c were missed. Of more importance is the fairly coarse detector segmentation as compared with other processor triggers.[3,4,5] This size causes a significant number of accidental tracks which occur when a road requirement is satisfied by unrelated detector hits created by several tracks. The system recovers from this problem in several ways. It uses fast ripple-through electronics so that the interesting tracks (as defined for a particular experiment) are recognized within 75ns as compared with the microseconds required by iterative search processors. This reduces trigger deadtime and allows analysis at a higher rate. By reporting measurements of kinematic quantities for

each track (i.e. (P,θ)) in addition to signalling simply the presence of some number of tracks[6], this processor allows a higher level trigger decision to be made.

In the present experiment the interesting tracks are kaons. However, the track finding is quite general, and the logic and detectors could be configured in such a way that the tracks of interest are muons, protons, etc.

A kaon is defined to occur when a road is satisfied and no cells in C2 which overlap this road have any light. The elements in H1 are placed so that in the small angle region, which has a high track density, they shadow the four-fold vertical segmentation of C2 and the horizontal segmentation of P3 (Fig. 3). With this arrangement, a kaon may be recognized even though a non-kaon (pion, etc.) shares the same road, if the two tracks are produced at sufficiently different vertical angles.

The resulting kaon definition logic is of the form

$$K(P,\theta) = P1_{\theta} \cdot \sum_{\mu=1}^{2} P2_{i(p,\theta,\mu)} \cdot P3_{j(p,\theta)} \cdot \sum_{\nu=1}^{4} (\overline{C2}_{k(j,\nu)} \cdot H1_{m(j,\nu)}).$$

The geometrical arrangement and Cerenkov threshold are such that kaons with momenta between about 6 GeV/c and 22 GeV/c are recognized.

As shown in Fig. 2, only the highest momentum track for each charge out for several that may have a given production angle is reported by the track finder to the higher level logic. This is the correct bias to use in this particular experiment where interesting tracks are kaons and a pion contamination exists near threshold in C2. This bias could easily be altered to benefit a different physics motivation, however.

Once the track recognition and momentum selection procedure is completed, the presence of a satisfied road with production angle θ and charge q is signalled to the higher level logic. The momentum corresponding to each road is also available for readout as needed by this logic.

IV. High Level Logic

A further trigger rate reduction is possible using the kinematic quantities (P, θ_x, θ_y) of interesting tracks found by the track finder. It is possible to compute values of variables such as effective mass and transverse momentum very rapidly using memory lookup techniques. In the $\phi\phi$ experiment a "kaon pair consistent with ϕ" determination was ready within 150ns of the time at which detector data was available to the processor.

For the $\phi\phi$ trigger it is desirable to choose two K^+K^- pairs with small opening angles between the K^+ and K^- within a pair. At the same time, since a large $\phi\phi$ effective mass is

wanted, a bias in favor of large opening angles between the pairs is imposed. This selection of tracks for calculational purposes is performed by the "select board" (Fig. 4).

The flags representing valid $K^{\pm}$ roads at various production angles θ are presented to a pair of 32-wide priority encoders. The outputs of these encoders are two five-bit words θ_L^+ and θ_R^+ which are the most positive and most negative production angles of all the satisfied positive kaon roads. Simultaneously, θ_L^- and θ_R^- are determined for the negative kaons. These four words are used to address the corresponding momenta determined in the road logic. Both the four momentum words S_L^+, S_R^+, S_L^-, and S_R^-, and the four words of θ are sent to the next module for use in the kinematic calculations.

These calculations are performed by a combination of arithmetic chips and PROMs loaded with functions, Fig. 5. It has been found that new proms can be burned very easily and quickly using the online computer. This strategy was adopted rather than the more common on of direct CAMAC/processor communication.

The effective mass of a pair of kaons is given approximately by

$$M_{KK}^2 \approx M_K^2 \left[2 + \frac{P_2}{P_1} + \frac{P_1}{P_2}\right] + P_1P_2 \left[(\theta_x^+ - \theta_x^-)^2 + (\theta_y^+ - \theta_y^-)^2\right],$$

assuming small angles and relativistic tracks. The trigger

processor could, in principle, calculate the effective mass of any pair of selected tracks. In this particular experiment, since low K^+K^- mass is required, and since the trigger rates are low, the approximation made is

$$M^2_{KK} \simeq P_1 P_2 (\theta^+_x - \theta^-_x)^2 = \frac{(\theta^+ - \theta^-)^2}{S^+ S^-} .$$

A kaon pair is accepted as a valid ϕ if M^2_{KK} as calculated is less than a Monte Carlo determined cut. In physical units the cut was at about 1.02 GeV/c. Since the processor uses only the bend plane opening angle and, therefore, always underestimates the mass, this cut is not unreasonably severe.

This processor also calculates the transverse momentum of the ϕ candidates in the xz plane as

$$PT = \left| \frac{\theta^+}{S^+} + \frac{\theta^-}{S^-} \right| .$$

Again, a complete three dimensional calculation for any pair of selected tracks is easily obtained but unnecessary in the present application. The resulting value is compared with a switch selected cut and an output is set "true" if the cut is passed. Both the mass and PT calculations are performed in parallel for the left and right ϕ candidate. To simplify timing of logic external to the processor, none of the high level decision outputs are set until the processor is strobed

by an external enable pulse.

V. Gating The Processor

Initial gating of the processor is provided by the IB, or interacting beam, signal which loads the latches (see Fig. 6). This signal is derived from the scintillation counters Si, i = 1,5 (Fig. 1). An incident beam track is defined by $B = S1 \cdot S2 \cdot \overline{S3}$ where S1 and S2 are upstream of the target and define the beam size, while S3 is an annular counter which vetos beam halo. The counter S5 is downstream of H1 and is used to require an outscattered beam particle. The counter S4 is directly downstream of the target, and the pulse height selection, $S4 \geq V = 3$ is used to require an interaction in the target.

In order to reduce the system deadtime a signal E = enable is then rapidly formed (within 50 nsec). If the event does not produce an E signal, it is aborted. The signal E consists of IB and $\overline{S4 \geq W = 15}$ and $\overline{C2 > Q = 5}$. The C2 multiplicity is derived from a commercial NIM module.

The signal E gates the Fermilab designed multiplicity window discriminators which produce a signal if the multiplicity N is between the limits, $N \equiv (NL, NH)$ or $NL \leq N \leq NH$. The six hodoscope multiplicites are used to form a signal EG (Event Gate) which is required in all subsequent trigger decisions. The logic schematic for the formation of EG and the trigger is shown in Fig. 7.

The hodoscope multiplicity distributions observed in this experiment are shown in Fig. 8. Note that the true reconstructed track multiplicity downstream of the magnet is ∿10, higher than the mean hodoscope multiplicity (∿7). The multiplicity limits are indicated on the Figure. The signal EG requires P1 = (N,M) = (4,9) · P2 = (N,M) = (4,9) · P3 = (N,M') = (4,10) · C1≤7 = P-1 · C2≤5 = Q-1 · H1≤6 = R-1. In addition, since the processor preferentially selects events where the Cerenkov counter C2 is inefficient, the multiplicity in C1 and in C2 is required to agree to within 2 = S-1.

The purpose of these gates is to select interactions in the target (IB) with limited multiplicity and not too many pions (E). A further refinement is to limit the processor multiplicity to prevent accidental K candidates and also to use C1 to limit the effects of C2 inefficiency (EG).

VI. Trigger Formation

The formation of the triggers is indicated in Fig. 7. The signal EG is required in all triggers. The processor, which is gated by the signal E, provides signals K^+ and K^-, the multiplicities of K^+ and K^- candidates, and ML and MR, signals which are valid if the leftmost and rightmost K^+K^- pairs have low masses in the magnet bend plane. In addition, the signals PTL and PTR, determinations of the transverse momenta of the leftmost and rightmost K^+K^- in the bend plane, are available for triggering purposes.

The trigger rates obtained in this experiment are given in Table 1. The trigger names correspond to the logic requirements:

$2K \equiv EG \cdot (K^+ = (1,4)) \cdot (K^- = (1,4))$

$\phi \equiv 2K \cdot (ML + MR)$

$\phi PT \equiv \phi \cdot (PTL + PTR)$

$4K \equiv EG \cdot (K^+ = (2,4)) \cdot (K^- = (2,4))$

$2K\phi \equiv 4K \cdot (ML + MR)$

$2K\phi PT \equiv 2K\phi \cdot (PTL + PTR)$

$\phi\phi \equiv 4K \cdot (ML \cdot MR)$

$\phi\phi PT \equiv \phi\phi \cdot (PTL + PTR)$

As can be seen in Table 1 the processor is a powerful tool in searching for rare processes. The reduction by track finding and multiplicity cuts is given by 4K/IB ∿ 1/300; the effect of high level calculations is $\phi\phi/4K \sim 1/8$.

The trigger rate for $\phi\phi$ was low enough, given the maximum beam flux that the detectors could tolerate, that the PTL and PTR signals were not used during the main data taking. The threshold values of PTL and PTR yielding the trigger rates of Table 1 correspond to 0.7 Gev/c in the magnet bend plane.

The results of the processor determination of K^+ and K^- multiplicity is shown in Fig. 9. Clearly, the number of kaon candidates falls rapidly with multiplicity. The cut for 4K triggers is shown in the figure. Also shown in Fig. 9 is the

correlation between K^+ and K^- multiplicity. Clearly if $2K^+$ are found, one is likely to find $2K^-$, as expected for real events.

A typical event display of a $\phi\phi$ trigger is shown in Fig. 10. Note that complex topologies are tolerable, as evidenced by the number of charged tracks in this event.

VII. K^+K^- Mass Measurement Using the Processor

The cut for triggering purposes was set at a limit of 8 processor mass units, i.e. ML = mL<8, MR = mR<8. The probability of occurrence of ML and MR in 4K events is shown in Fig. 11a. The positive value of the correlation function indicates that if the processor detects an ML signal it is likely to also detect an MR signal. This is expected since $\phi\phi$ production is known to be correlated.[7]

By utilizing the latched hodoscope information one may study details of the mass distributions online. In Fig. 11b is shown the probabilities of mL and mR for $\phi\phi$ triggers. Clearly a band exists for low mL and mR values. In Fig. 11c is shown the Monte Carlo result for the expected m distribution for $\phi\phi$ events. Note that, since ~50% of all $\phi\phi$ events yield m<2, the trigger cut of 8 mass units is conservative.

In Fig. 11d a crude background subtraction is shown. Events with 0<mL<2 are plotted vs. mR along with events with 4<mL<6, assumed to be background, normalized to equal rates for 4<mR<6. An excess of events remains at low m_R, corresponding to the existence of $\phi\phi$ events. The very fact that $\phi\phi$ events can

be seen online at the trigger level indicates the discrimination power of this trigger processor for rare event topologies.

VIII. Offline Reconstruction of $pp\to K^+K^-K^+K^- + n\pi$ Events

Final proof that the processor is working requires three dimensional reconstruction of the events which triggered and the observation of correlated low mass enhancements.

For comparison purposes, the best previous published high energy experiment[7] obtained 112 $\phi\phi$ events for 4×10^6 triggers, or $\phi\phi$/trigger = 1/36,000. In Fig. 12a a scattergram of $M(K^+K^-)_L$ vs $M(K^+K^-)_R$ is shown for events reconstructed from 90,000 triggers. In Fig. 12b the background due to $K^+K^-K^+K^-$ events is roughly subtracted leaving 571 ϕK^+K^- and 379 $\phi\phi$ events. In Fig. 12c the ϕK^+K^- background is crudely subtracted leaving 233 $\phi\phi$ events, or $\phi\phi$/trigger $\geq$ 1/400. This number is somewhat worse than that inferred from Fig. 10 which used the hodoscope bits online to estimate the trigger purity. Note that, since the analysis programs are not yet optimized, the quoted value for $\phi\phi$/trigger is a lower limit.

The final result of this analysis is that the trigger processor allows one to study a rare process such as $pp\to\phi\phi x$ at least two orders of magnitude more cleanly than any previous experiment. As experiments in general search for ever rarer reactions, this analysis indicates the power of and need for subtle and sophisticated trigger processors.

IX. Acknowledgements

The authors wish to thank a number of people and institutions who supported the work described in this report both financially and by aiding in the construction and design of the devices. A.E. Pifer is responsible for the successful operation of the CAMAC/PROM interface. J. Albright and F. Rydeen and his staff helped with the construction of the scintillator hodoscope and electronic assembly. H. Goldman and J. Marraffino worked diligently to provide off-line analysis both during and after the experimental run. Many others provided support funded by the U.S. Department of Energy (University of Arizona: AC02-80ER10663, Florida State University: AS05-76-ER03509, and Tufts University: AC01-76-ER03023) and the U.S. National Science Foundation (University of Arizona: PHY-79-08641, University of Notre Dame: PHY-81-12897, Vanderbilt University: PHY-81-21161, and Virginia Polytechnic Institute: PHY-80-20441).

REFERENCES

[1] MUPAC Coprporation, Brockton, MA, U.S.A.

[2] William R. Blood, Jr., MECL System Design Handbook, (Motorola, Inc., U.S.A., 1980).

[3] J. Martin, et al, FERMILAB-Conf-81/40-EXP

[4] T. F. Droege, I. Gaines, and K. J. Turner, IEEE Trans. Nucl. Sci. NS-25, 698 (1978).

[5] F. Bourgeois, IEEE Trans. Nucl. Sci. NS-27, 594 (1980).

[6] A. Etkin, et al, Phys. Rev. Lett. 40, 422(1978).

[7] C. Daum, et al, Phys. Lett. B 104,246(1981).

TABLE 1

TRIGGER RATES

NAME	σ (μb)
IB ≡ σ_I	30,000.
E	8,760.
EG	1,077.
2K	377.
φ	121.
φPT	60.
4K	94.
2Kφ	51.
2KφPT	26.
φφ	12.
φφPT	4.

FIGURE CAPTIONS

1) Plan view of the trigger detectors and a block diagram of the trigger electronics.

2) Logic system which defines one road and the system for reporting the momentum of selected roads.

3) View along the beam direction of the small angle region of H1, C2, and P3 showing the horizontal and vertical relationship of the detector elements. Also shown is the logic used to select kaons in this busy region.

4) Block diagram of the logic that chooses roads to be used as left and right kaon pairs and causes the corresponding measurements of P and θ to be used in the kinematic calculations.

5) Schematic of the logic used to calculate mass and transverse momentum.

6) Schematic diagram of the logic for generation of the signals IB and E.

7) Schematic diagram of the logic for generation of the signal EG and of the logic for usage of processor signals, K^+, K^-, ML, MR, PTL, and PTR, in formation of the final trigger. Window discriminator cuts are indicated using notation defined in the text.

8) Hodoscope multiplicity distributions for the six detectors used in the trigger.

   a) P1 b) C1 c) P2 d) C2 e) P3 f) H1

   Trigger limits are indicated by the arrows.

9) Processor selection of kaons.

   a) The correlation function for correlations between the K^+ multiplicity and the K^- multiplicity found by the processor.

   b) Multiplicity distributions for the number of K^+ and K^- found by the processor. Trigger cuts are shown as arrows.

10) Diagram of an event selected by the processor. Struck trigger hodoscope elements as well as hits in other detectors are indicated. Solid lines represent the four tracks that triggered the system. Dashed lines indicate the extra tracks tolerated by the processor.

11) Processor determination of masses.

a) Correlation function for ML, MR using 4K triggers.

b) Distribution of mL and mR within the trigger cut for $\phi\phi$ triggers. The tabulated numbers are the fraction of $\phi\phi$ triggers yielding a particular mL and mR.

c) Monte Carlo generated distribution of the expected processor mass for ϕ events.

d) Background estimation in $\phi\phi$ triggers. A column of b) expected to contain $\phi\phi$ events (solid lines) is shown along with a column expected to contain background (solid circles), normalized to the same area for mR>4. Also shown is the expected residual shape due to ϕ events (open circles) using the shape of c).

12) A scattergram of reconstructed $K^+K^-K^+K^-$ + nπ final state events.

a) $M(K^+K^-)^L$ vs $M(K^+K^-)^R$

b) Estimated $K^+K^-K^+K^-$ background subtraction.

c) Estimated ϕK^+K^- background subtraction.

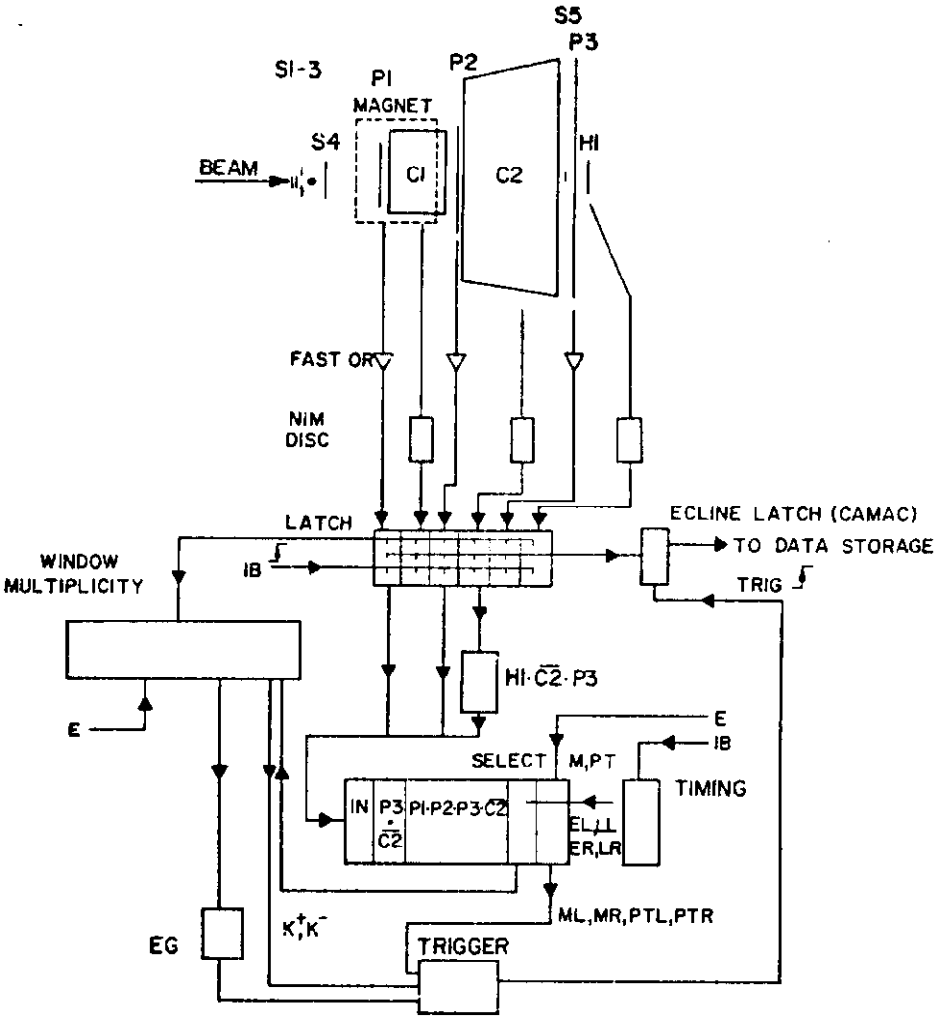

Fig. 1

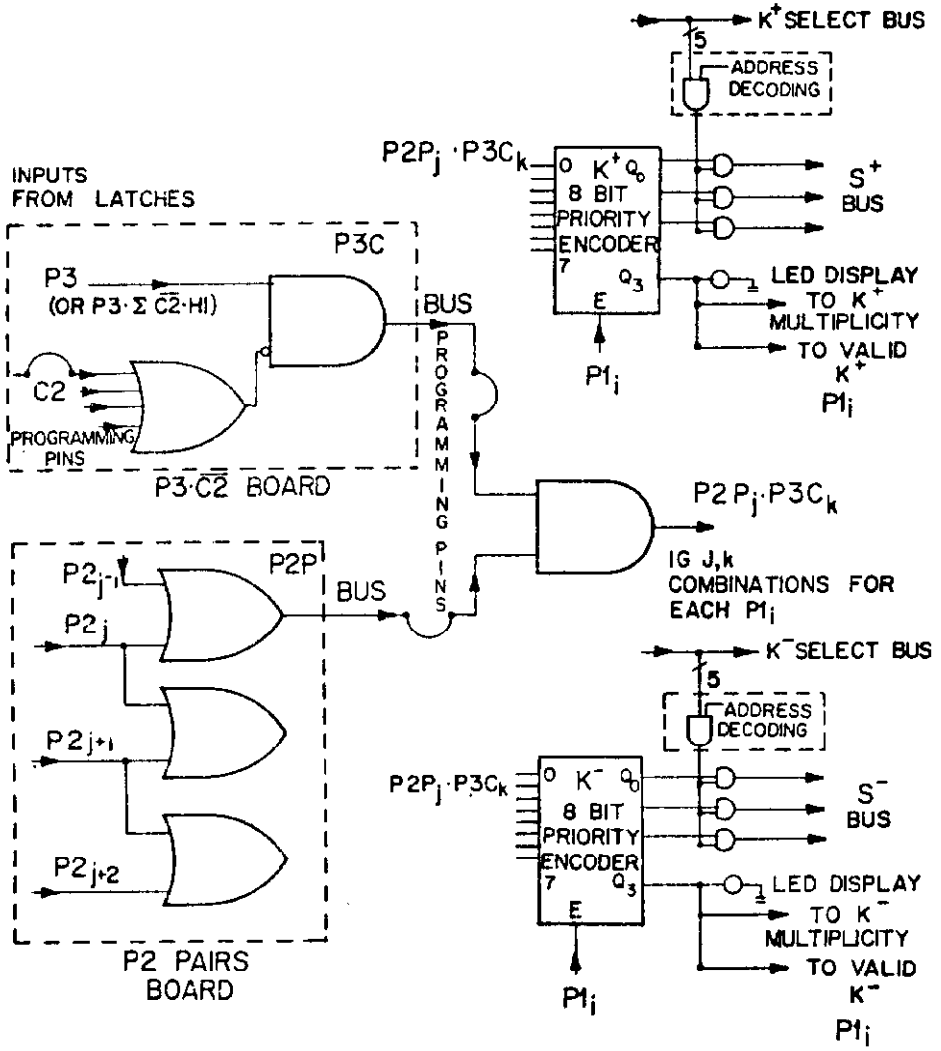

Fig. 2

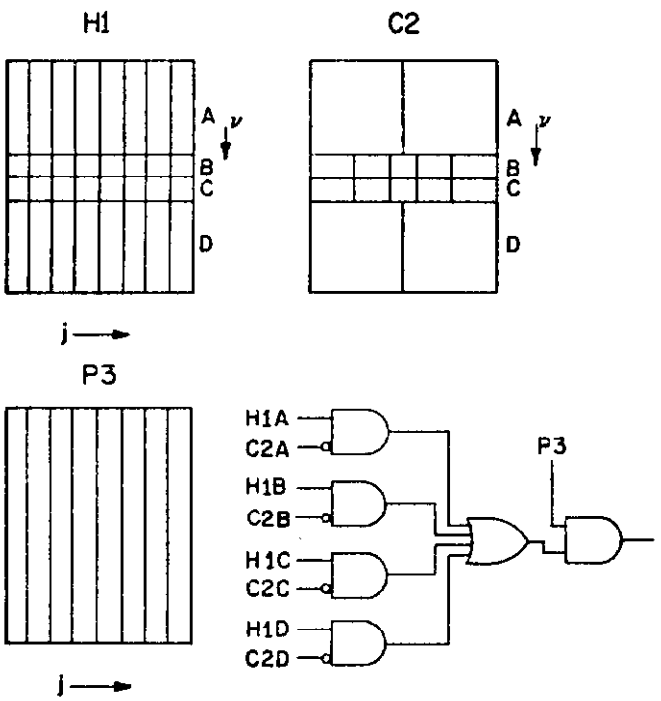

$$P3_j \cdot \sum_{\nu=1}^{4} (\overline{C2}_{k(j,\nu)} \cdot H1_{m(j,\nu)})$$

Fig. 3

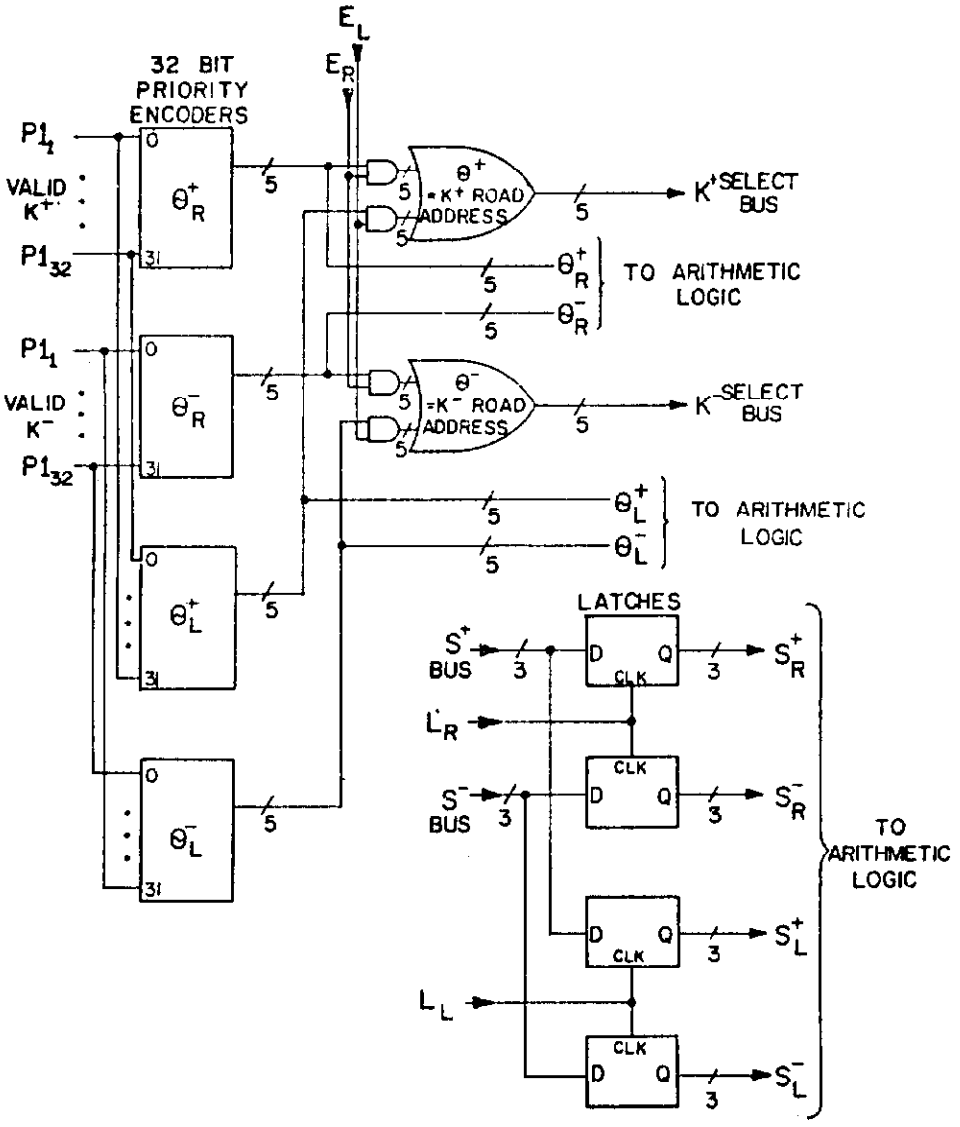
32 BIT
PRIORITY
ENCODERS
VALID
TO ARITHMETIC
LOGIC
SELECT
BUS
LATCHES
CLK
TO
ARITHMETIC
LOGIC

Fig. 4

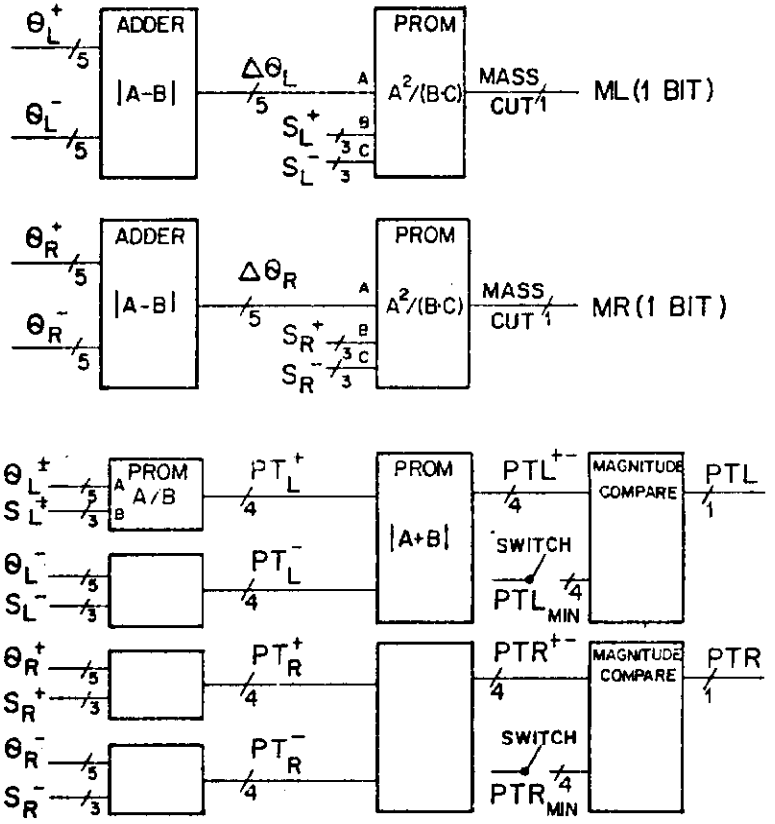
ADDER
|A-B|
PROM
MASS
CUT
ML(1 BIT)
MR(1 BIT)
PROM
A/B
|A+B|
SWITCH
MAGNITUDE
COMPARE

Fig. 5

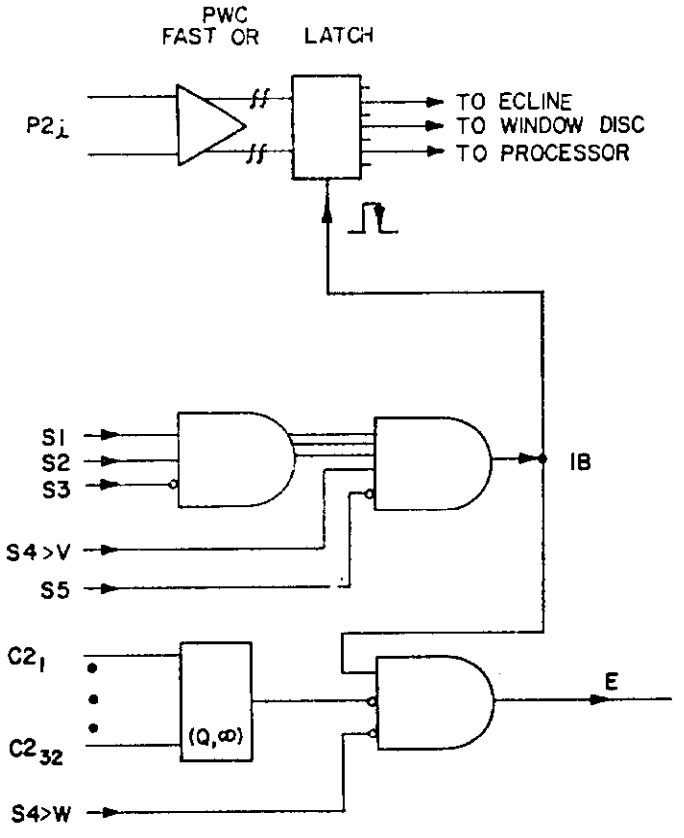
PWC
FAST OR
LATCH
P2i
TO ECLINE
TO WINDOW DISC
TO PROCESSOR
S1
S2
S3
S4>V
S5
IB
C2₁
C2₃₂
(Q,∞)
E
S4>W

Fig. 6

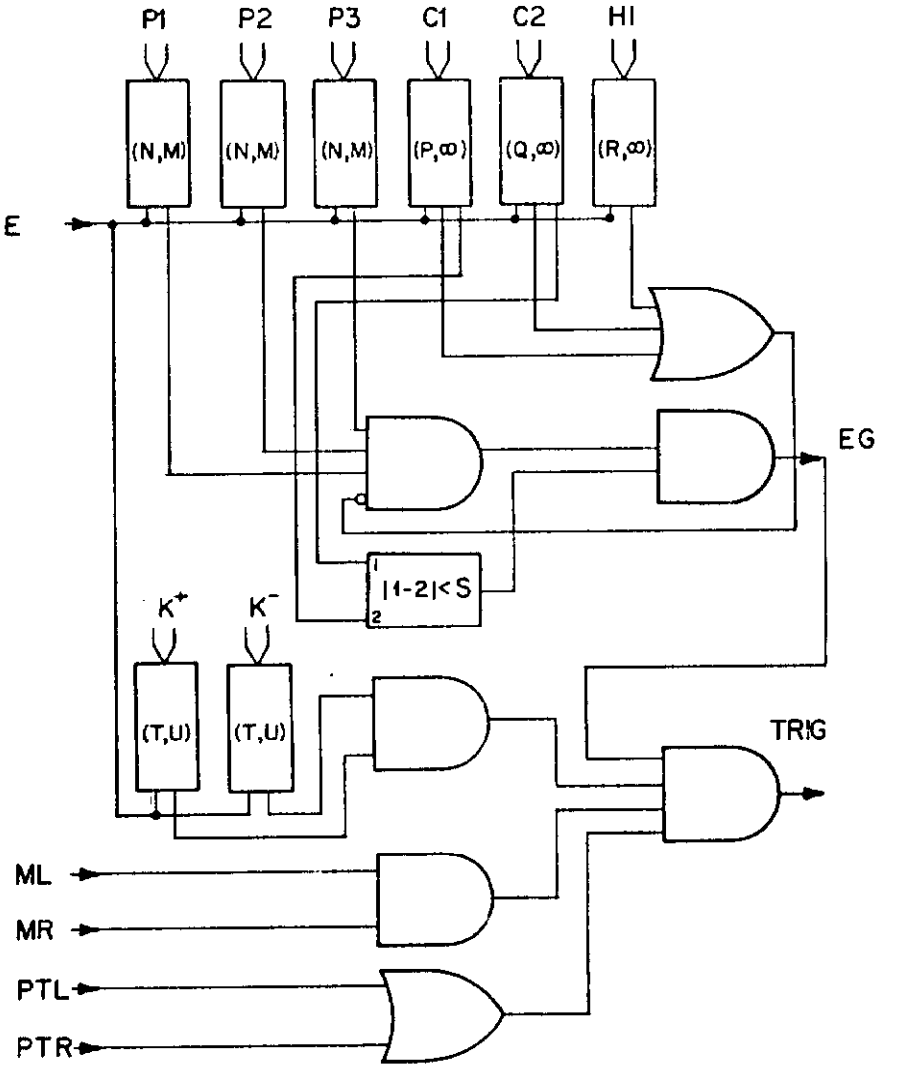
P1
P2
P3
C1
C2
HI
(N,M)
(N,M)
(N,M)
(P,∞)
(Q,∞)
(R,∞)
E
EG
|1-2|<S
K⁺
K⁻
(T,U)
(T,U)
TRIG
ML
MR
PTL
PTR

Fig. 7

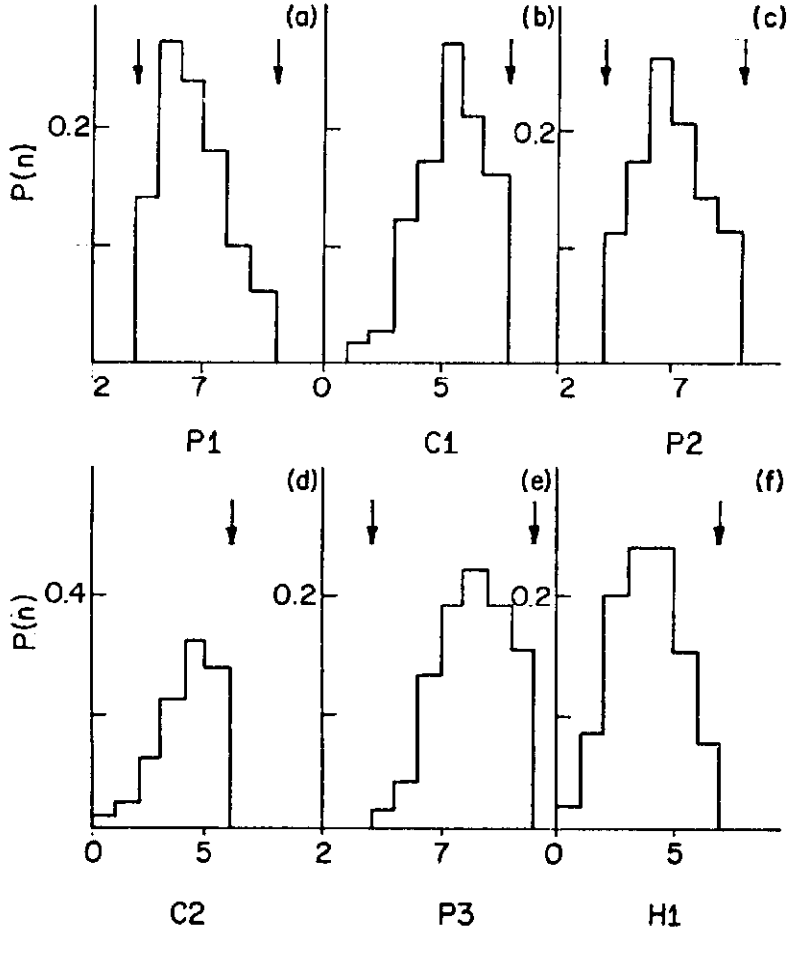

Fig. 8

$K^{\pm}$ DETERMINATION

a)

N_{K^-} \ N_{K^+}	0	1	2
0	-.025	-.16	-.003
1	-.20	.082	.23
2	-.059	.23	.32

$$\left[(P_{+-})-(P_{+})(P_{-})\right]/(P_{+})(P_{-})$$

b)

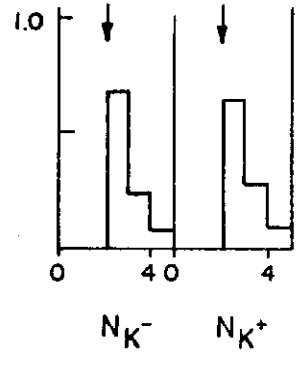

Fig. 9

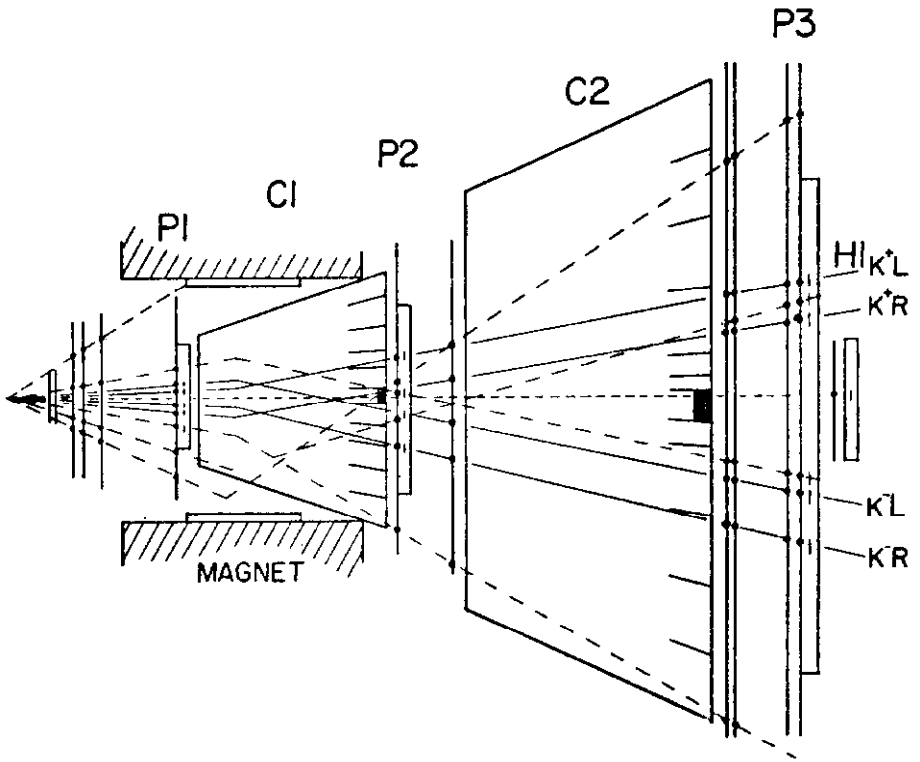

Fig. 10

K^+K^- MASS DETEMINATION

a)

P(ML) = .22
P(MR) = .20
P(ML·MR) = .083

$$\frac{P(ML\text{-}MR) - P(ML)\,P(MR)}{P(ML)\,P(MR)} = 0.89$$

b)

mR \ mL	0	2	4	6
8	.047	.029	.028	.028
4	.075	.044	.048	.029
2	.088	.056	.040	.029
0	.18	.090	.077	.049

c)

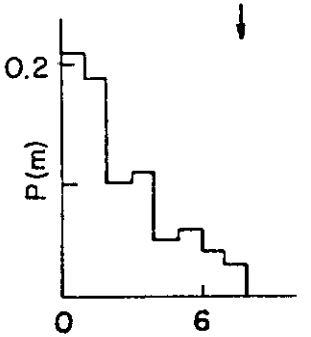

d)

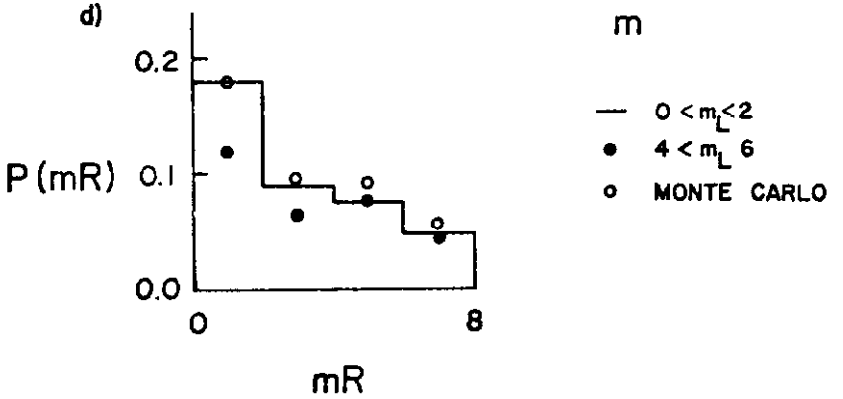

Fig 11

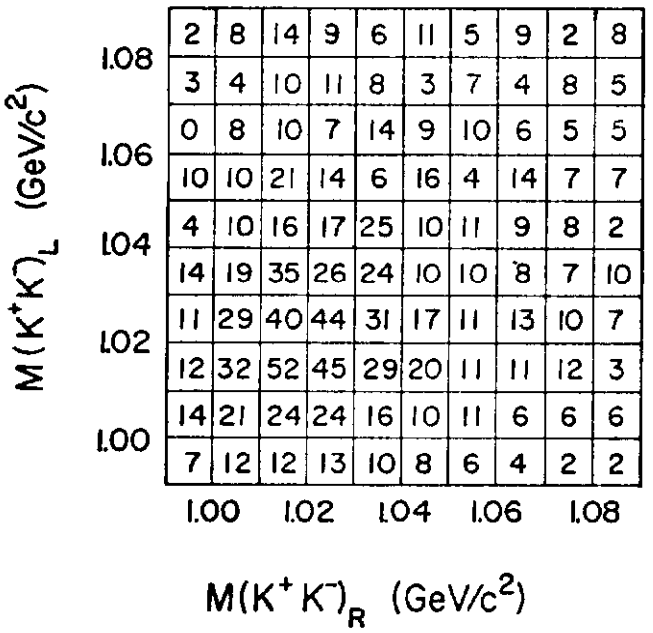

Fig. 12a

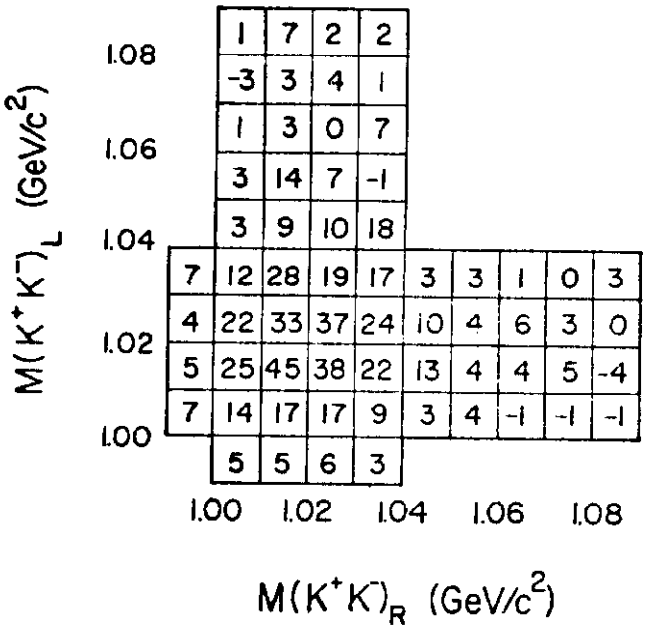

Fig. 12b

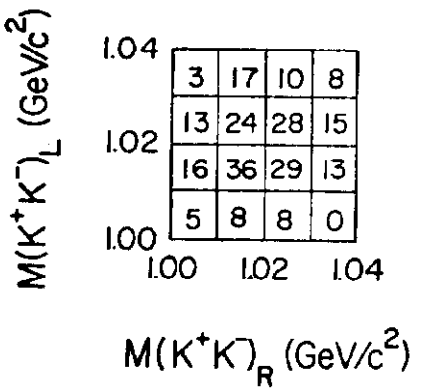

Fig. 12c